Bottom Currents near a Small Hill on the Madeira Abyssal Plain

PETER M. SAUNDERS

Institute of Oceanographic Sciences, Wormley, Godalming, Surrey, UK

(Manuscript received 8 September 1987, in final form 4 December 1987)

ABSTRACT

Near-bottom currents at depths in excess of 5000 m have been measured in the Great Meteor East study area (near 31°30'N, 25°W) over a 3 year period. The sites selected were on top of a small abyssal hill, on its flank, and on the abyssal plain 30 km distant from the hill. The magnitude of the mean current 10 m above the seabed was 1–2 cm s^{-1} but its direction was quite different at the three sites and reflected the presence of a clockwise vortex trapped over the hill. On the plain the mean flow direction was to the west and directly opposed to that furnished by a β-spiral analysis of the density field. It is suggested that time dependent variations in the large-scale density field are more important than hitherto supposed.

For periods greater than 120 days the variance of the current on the plain is concentrated in the east component, and for periods 50–120 days the variance is concentrated in the north component. Fluctuations propagate *westward* at speeds 1–10 cm s^{-1} but are more complex than barotropic planetary waves. From estimates of the integral time scale of these motions (6–14 days) horizontal diffusivities of between 2 and 5 ($\times 10^2$ m^2 s^{-1}) have been deduced.

Estimates of the abyssal vertical velocity on the flank and top of the hill reveal the influence of the slope of the local bottom; on the plain any signal is buried in measurement noise.

1. Introduction

Currents have been measured for a three-year period near the seabed in the northeast Atlantic. The observations were made as part of a study to assess the feasibility of disposing of high-level radioactive waste in the sediments of the deep ocean. The area was selected for the suitability and stability of its sediments (Searle et al. 1985) and was near the location 31°30'N, 25°W; it was designated Great Meteor East (GME).

A review of current measurements made up to 1984 (Dickson et al. 1985) revealed that, in the general area of GME, deep currents were weak but that none of the measurements had a duration sufficient to establish the mean flow. Once the site of the study area was selected a new programme of current measurements was devised with the following objectives:

1) to establish the climatology of currents on the Madeira abyssal plain and to estimate their dispersion, and

2) to deduce the effect of a neighbouring 400 m-high hill on these currents and on their dispersion.

In addition to the moored current meter measurements a group of nine free drifting SOFAR floats were released at a location 100 km NE of the GME site. The floats were ballasted for 3000 m depth and their dispersion was measured over the same period: it is hoped to report on these at a later date.

Corresponding author address: Dr. Peter M. Saunders, Institute of Oceanographic Sciences, Brook Road, Wormley, Godalming, Surrey, UK GU8 5UB.

2. The site for measurements

The Great Meteor East study site lies on the Madeira abyssal plain in the center of the Canary Basin. To the west the abyssal plain abuts against the lower flank of the Mid-Atlantic Ridge, and is characterized by the outcropping of abyssal hills elongated in the SW–NE direction (Searle et al.). To the east the abyssal plain merges smoothly into the deepest parts of the lower continental rise and to the north the basin is bounded by the Azores–Gibraltar rise. The local and regional bathymetry is shown in Fig. 1. At GME the water depth on the abyssal plain is approximately 5440 m and an unnamed abyssal hill at 31°30'N, 25°10'W has a minimum depth of just less than 5000 m and hence a height of 450 m above the plain.

Three sites were selected for long-term current measurements:

(i) on the plain about 30 km from the nearest hill and representative of the abyssal plain
(ii) on the summit of the small hill
(iii) at the foot of the same hill,

the last two to determine the effect of the hill on the flow. A short duration current measurement was also made at 31°17'N, 25°24'W.

Three current meters were installed on the long-term moorings. The first was 10 m above the seabed and the

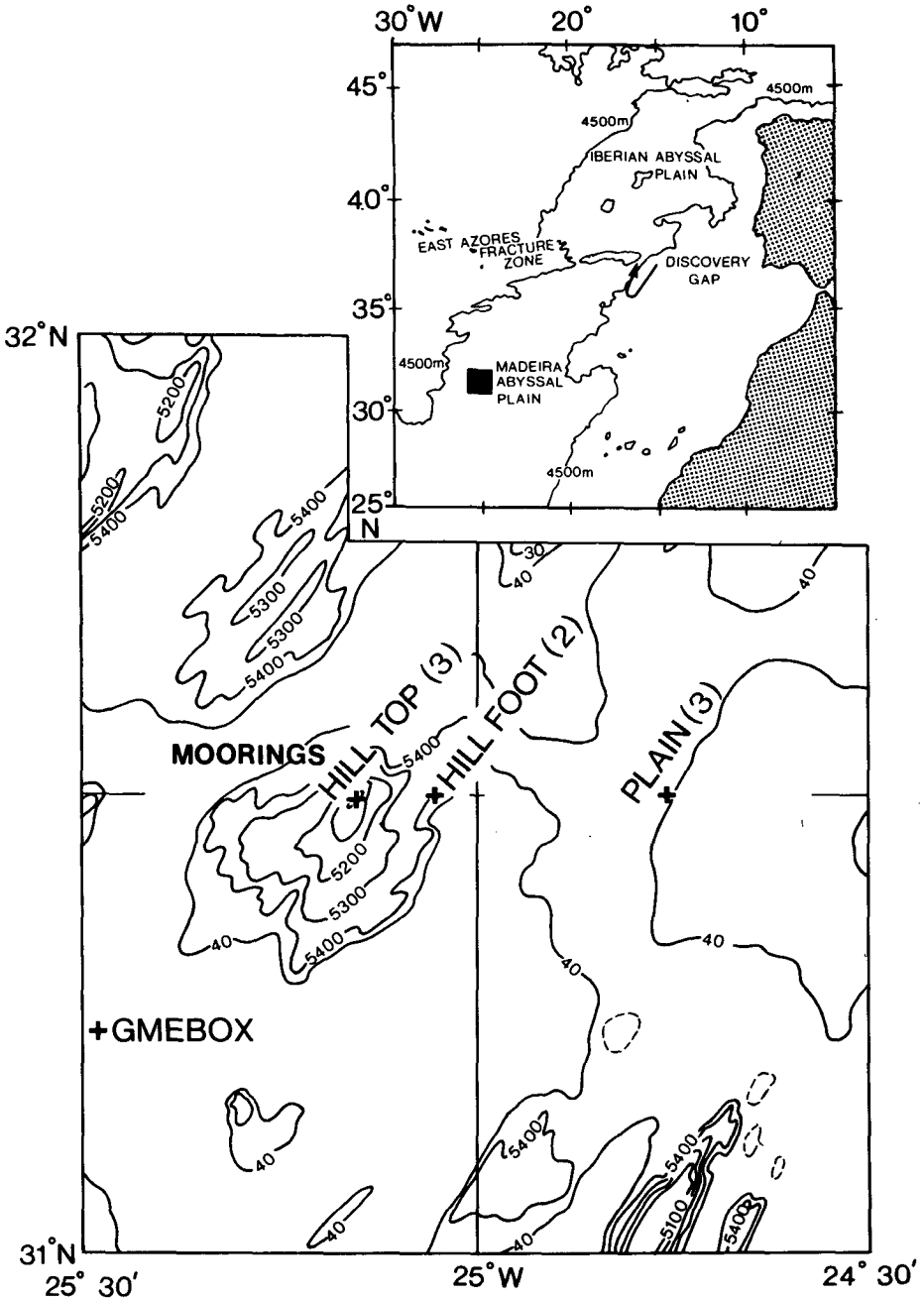

FIG. 1. Map of Great Meteor East study site showing mooring locations: in parenthesis number of successful recoveries.

second was 1000 m above this; the latter instrument to learn something about the vertical structure of near-bottom currents. A third instrument, 100 m above the bottom, was introduced primarily for redundancy. Thus three moorings were deployed, one at each of the above sites, with three instruments on each (Fig. 2). Such moorings have a safe lifetime of about 1 year and three deployments were made to cover the period from 30 January 1984 to 24 September 1986.

3. Instrumentation, moorings and data quality

The data were gathered at hourly intervals utilizing Aanderaa RCM5 current meters. Instruments were individually calibrated for rotor speed, compass direction, and temperature. The rotor stall speed lies between 1.5 and 2.0 cm s^{-1} and direction values are reproducible in pre- and post-cruise calibrations to within ±3°. The temperature circuits had been modified (Saunders and

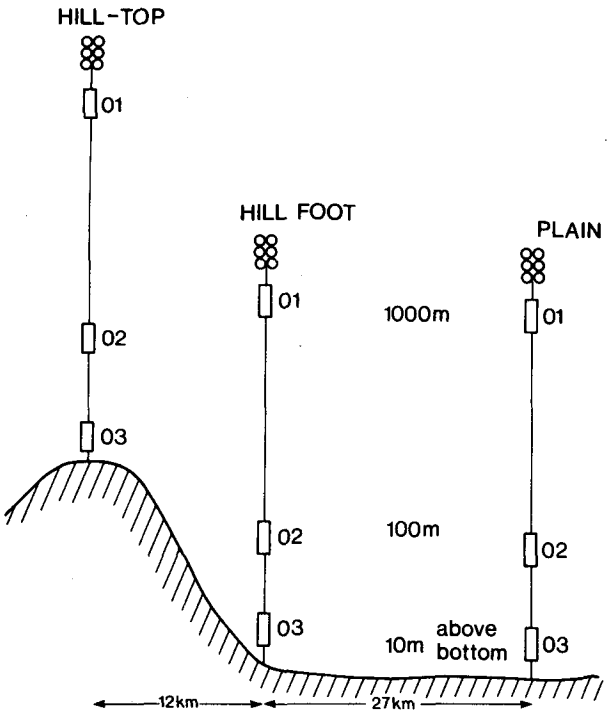

FIG. 2. Schematic cross section of the three moorings and nine current meters utilized in this paper.

Cherriman 1983) to yield a sensitivity of 0.0025°C per count.

Moorings were of 10 and 12 mm braided polypropylene with 300 kg of chain anchor and six 17-inch diameter Benthos glass spheres, which provided 150 kg of buoyancy; acoustic releases were of IOS design. The weak currents ensured that knockdown of the moorings were negligible (<10 m).

Mooring locations at the sites occupied at GME are presented in Table 1. Details concerning the individual current meter records (duration of each deployment, depth, data return) are available in report form (Saunders 1987a) and will not be reproduced here. In all, 28 instruments were deployed for an expected duration of 8770 days but only 7346 days or 84% of the data were recovered. The severest loss was of mooring 399 which we suppose pre-released, surfaced and drifted away. So far, it has not yet been recovered.

The processing of the data is described in Saunders (1987a). Here we note that because of very weak currents the rotor is commonly stalled, see Table 2. It is IOS practice to set the current speed equal to the stall value at this time[1]; it will be confirmed in subsequent tables that the difference resulting from IOS standard practice and setting the value equal to zero is very small. Most of the important conclusions result from the energetic events (strong currents) for which the very weak current treatment is irrelevant.

The hourly mean rotor speeds of 3–4 cm s^{-1} are primarily the consequence of the semidiurnal tide.

[1] It is unusual for the vane to be stalled when the rotor is stalled: setting the speed zero discards the directional information when components are computed.

TABLE 1. Mooring locations. The deployment at the first three sites was from 30-I-84 to 24-IX-86: and at the last from 19-VIII-85 to 19-XI-85.

Site	Mooring	Latitude (°N)	Longitude (°W)	Depth (m)
Plain	365	31 31.3	24 45.4	5438
	391	31 30.2	24 45.2	5438
	400	31 28.8	24 43.8	5444
Hill-foot	366	31 31.1	25 01.1	5398
	389	31 30.4	25 03.1	5433
	399*	31 32.4	25 01.0	5444
Hill-top	367	31 29.7	25 09.6	4999
	387	31 29.2	25 08.4	4989
	401	31 29.4	25 08.5	5055
GME box	—	31 14.9	25 26.6	5450

4. The interaction of the abyssal hill with the flow

The mean currents at heights 10 and 1000 m above the seabed at each of the three sites are shown in Table 3: they have a magnitude of between 0 and 2 cm s^{-1} and in the lowest 100 m quite different directions at the three sites (Fig. 3). On the plain the mean flow is west, at the hill-foot it is south and on the hill-top east; because the 10 and 100 m results are so similar the latter is ignored in this and ensuing sections. These measurements confirm the weakness of the abyssal mean flow in the GME area. The impact of the manner in which periods of stalled rotor are treated is illustrated for the observations made on the plain. Where the current is assumed zero when the rotor is stalled the record

TABLE 2. Hourly mean speeds and percent stall, by deployment.

Site	Height above bottom (m)	Mean speed (cm s^{-1}) 1	2	3	Percent stall 1	2	3
Plain	1000	2.90	3.24	3.32	52	44	61
	100	4.03	3.24	3.86	14	42	32
	10	3.97	3.69	3.58	16	31	38
Hill-foot	1000	3.87	3.91	*	22	18	*
	100	4.56	3.96	*	12	21	*
	10	4.22	*	*	19	*	*
Hill-top	1000	3.16	3.98	*	35	23	*
	100	3.75	4.09	4.25	24	26	15
	10	4.04	4.13	4.28	19	24	19
GME box	3	*	4.30	*	*	18	*

TABLE 3. Experiment mean currents. Components which are bold are reliable (see text). Figures in parentheses are calculated with stalled rotor currents set at zero.

Site	Height above bottom (m)	Mean speed (cm s^{-1}) East	Mean speed (cm s^{-1}) North	Speed (cm s^{-1})	Direction (°T)	Duration (days)
Plain	1000	**−0.71 (−0.57)**	−0.16 (−0.19)	0.73 (0.60)	257 (252)	963
	10	**−0.80 (−0.69)**	−0.02 (−0.08)	0.80 (0.69)	268 (262)	963
Hill-foot	1000	−0.04	−0.82	0.82	183	267
	100	−0.49	**−1.97**	2.03	194	651
Hill-top	1000	−0.05	−0.12	0.12	207	570
	10	**1.34**	−0.19	1.35	098	960

mean values are only approximately 1 mm s^{-1} less than those calculated for our "standard" treatment of stalled data.

The reliability of the above component mean values can be assessed from the approximate expression for the squared error (Bendat and Piersol 1971)

$$\epsilon^2 = \frac{2\sigma^2 I}{T}$$

where σ^2 is the variance of the east/north component about the mean, T is the record duration and I is the integral time scale. The computation of integral time scale is described in section 7 on current dispersion; here a value of 10 days is assumed. Given $\sigma \approx 2.5$ cm s^{-1}, for record durations of 250, 650 and 950 days the errors are 0.7, 0.45 and 0.35 cm s^{-1}, respectively. In Table 3 the components printed bold are larger than the error estimates given above.

The lack of reliability in estimating mean currents arises, of course, from the unsteadiness of the flow which is reflected in the value of σ. This unsteadiness

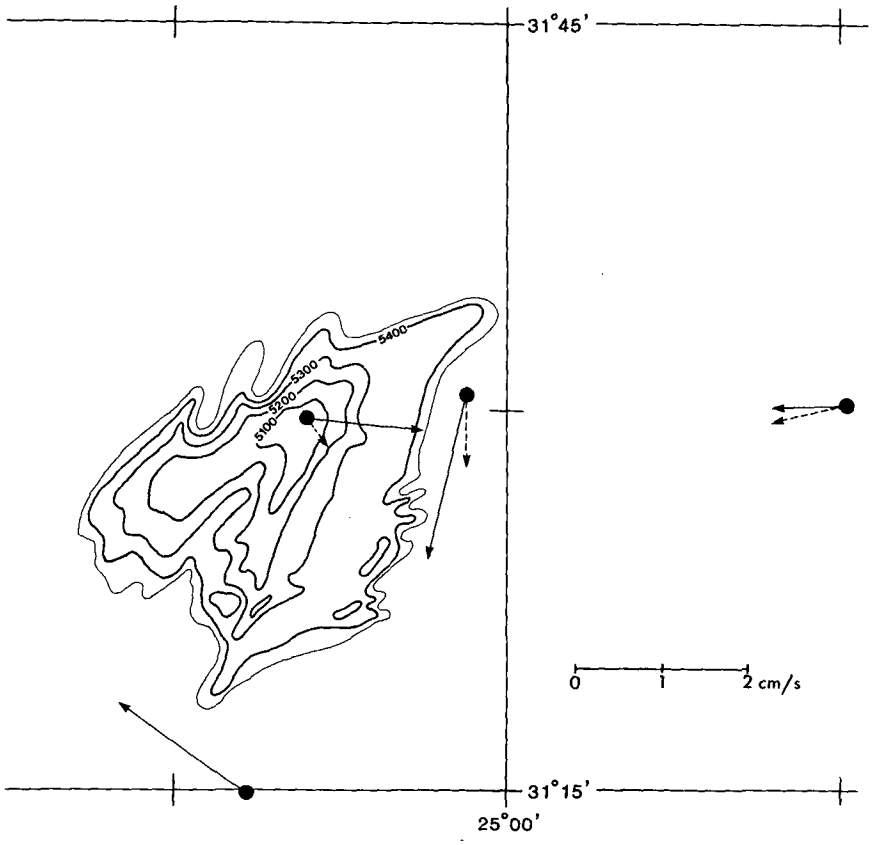

FIG. 3. Record mean currents at 10 m (solid) and 1000 m (dashed) above seabed.

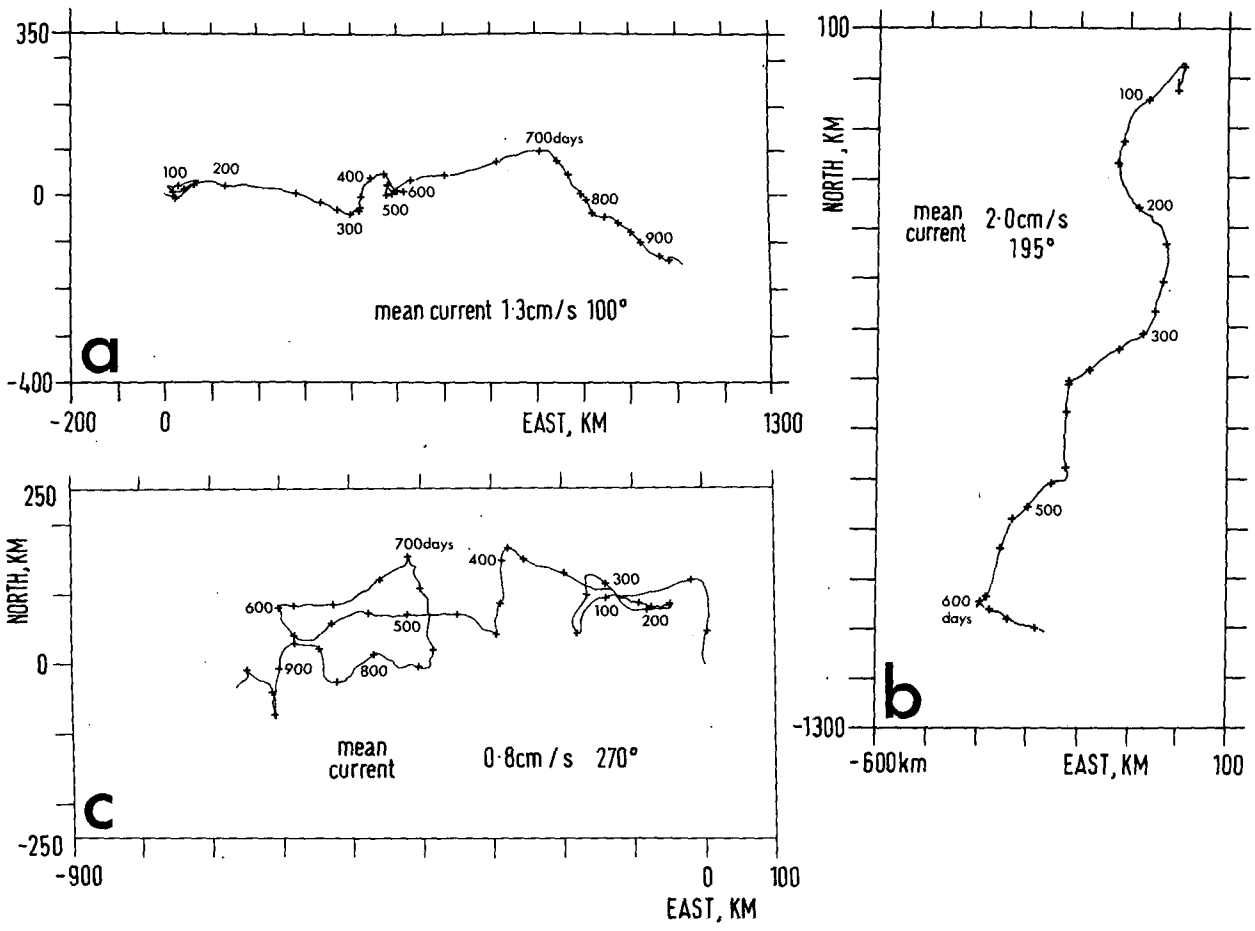

FIG. 4. Virtual displacement of water 10 m above bottom at the three sites: 25 day intervals are indicated as +. (a) hill-top, (b) hill-foot, (c) plain.

is readily illustrated (Fig. 4) by calculating the virtual displacement resulting from an integration of the current. Figure 4c shows the 10 m currents on the plain, the most unsteady of the three, with long periods (50 days) of flow reversal. Figure 4b shows 100 m currents at the hill-foot; while the mean direction closely parallels the nearby contours (Fig. 3) there are numerous periods of both off-hill and on-hill flow. Figure 4a shows 10 m currents on the hill-top; there are periods of near stagnation with bursts of strong easterly flow. The estimates of error in the components indicated above, when taken with the mean values from Table 3, yield directional uncertainties for the currents near the seabed. For the plain these are ±25°, and for the hill-foot and hill-top ± 15°. Evidently the directions of the mean flow at the three sites are significantly different from one another.

The explanation for these differences is to be sought in the presence of the abyssal hill itself. Two experiments have been performed in the deep ocean to study the influence of an abyssal hill on the nearby circulation (Gould et al. 1981; Owens and Hogg 1980) and both theoretical (Huppert 1975) and numerical results (Huppert and Bryan 1976) were invoked to interpret the observations.

The measurements at GME confirm the picture so far derived. A vertical uplifting of isothermal surfaces over the hill is seen (Fig. 5). This effect decays approximately exponentially with height (Owens and Hogg 1980, p. 1032) with a vertical scale H_s given by

$$Lf/\bar{N}$$

where L is the horizontal scale of the hill (10 km), f the Coriolis parameter and $\bar{N}$ the Brunt–Väisälä frequency (averaged over the depth H_s, approximately). The expected decay with height is confirmed in Fig. 6 (right). The parameter $\bar{N}h/U$, where h is the height of the hill and U the oncoming current strength, has a value of about 10 which ensures (Huppert and Bryan) that a clockwise (in the northern hemisphere) vortex is trapped on the hill. From the compression of isotherms and conservation of potential vorticity, the relative vorticity ζ in the vortex can be computed (Fig.

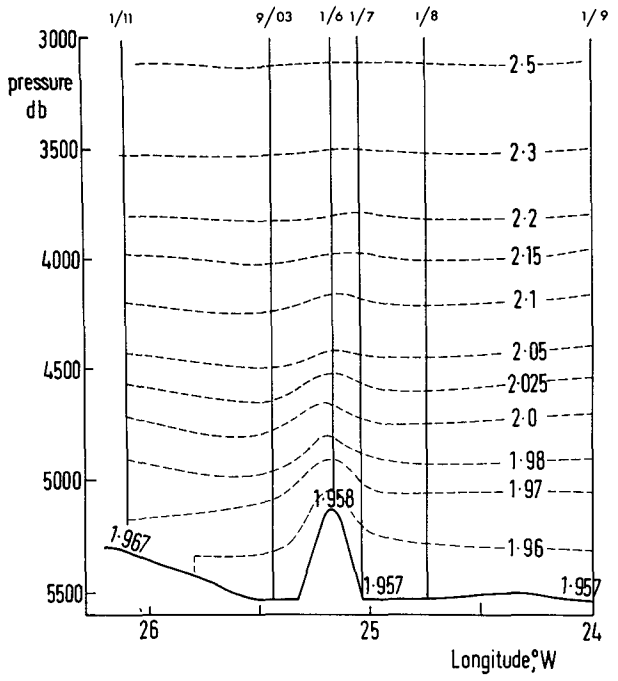

FIG. 5. E–W section of potential temperature versus pressure (depth) on 31°30′N: note the doming of the isotherms over the hill.

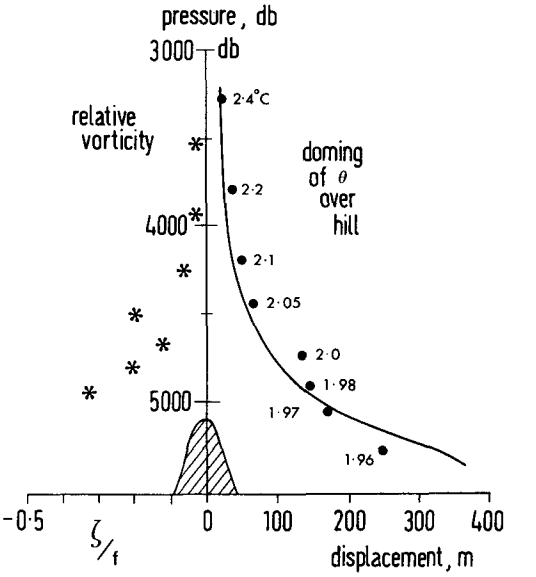

FIG. 6. Decay of influence of hill with height above it. (Left) relative vorticity in the swirling flow; (right) doming of isotherms revealed by data (●) and theory (line).

6, left). The maximum value ζ/f is found to be of the order h/H_s—considerably larger than that, h/D where D is the fluid depth, arising in an unstratified fluid.

The interaction of the trapped vortex and the oncoming flow leads to an asymmetry in the circulation; looking downstream from upstream of the hill the flow is intensified on the left flank and weakened on the right (Huppert et al.). In the report by the author cited earlier, 25-day segments of the flow were selected to illustrate this effect: they are long enough ($\gg L/U$) that the steady solutions apply. Periods were chosen when the flow direction on the plain arrived from the cardinal points. When the flow on the plain is from the east (west), the "hill-foot" mooring is 10 km upstream (downstream) from the top of the hill and the "hill-top" mooring is about 1 km from the top of the hill on its right (left) flank. When the flow on the plain is from the north (south) the hill-foot mooring is now at 10 km distance on the left (right) flank of the hill and the hill-top mooring 1 km upstream (downstream). All such situations, including intermediate flow directions are superimposed in Fig. 7 by rotating the plotted current vectors and their sites about the top of the hill in order to bring the flow at the "plain" mooring (not shown in Fig. 7) into a common westward direction. The persistence and ubiquity of the clockwise vortex trapped on the hill is displayed in striking fashion.

One must be cautious of interpreting this figure as a spatial description of the mean flow since two assumptions are tacitly made, viz. that the hill is symmetric and that the off-hill flow is uniform on the scale of about 50 km. Neither assumption is well-founded. Nevertheless the above strategy illustrates how a limited number of observing sites might be employed to calculate the bottom-stress or torque exerted by a small symmetric topographic feature.

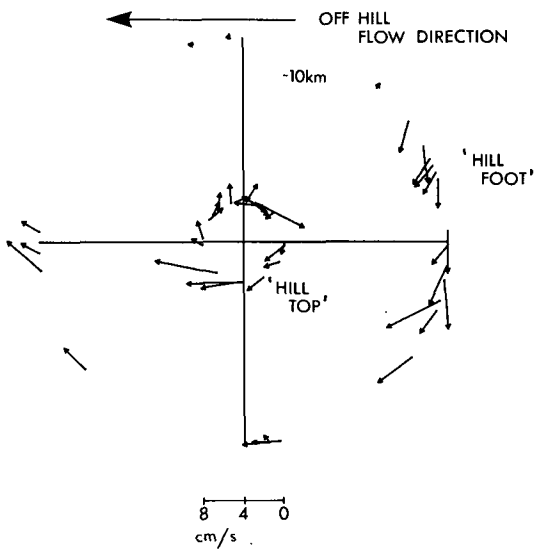

FIG. 7. Superposition of 20-day average current vectors measured at the hill-foot and hill-top sites. At both these sites and also on the plain (not shown) the current vectors are rotated about the center of the hill to bring the flow on the plain into an east–west direction.

The explanation of the mean flow at the three sites now becomes evident. The westward flow on the plain is the flow undisturbed by the effect of the topography; the two other long-term sites both reveal the swirling anticyclonic flow over the hill. As noted earlier the hill-top site lies north of the highest point of the hill: its eastward mean is substantially derived from the intense bursts which accompany the eastward flow on the plain. Such intense flow is not seen 1000 m above the seamount and the mean there cannot be distinguished from zero.

5. The mean flow on the plain

Away from topography the flow on the plain is found to be westward. The northward component is small and cannot be distinguished from zero but the east component is $-0.8, -0.8, -0.9 \pm 0.35$ cm s^{-1} at heights of 1000, 100 and 10 m above the seabed.

A persistent flux of water at depths between 4000 and 5000 m has been measured to pass from the Madeira Basin into the Iberian Basin to its north (Saunders 1987b). The flow passes through Discovery Gap (Fig. 1) and its magnitude $\sim 5 \times 10^5$ m^3 is such that if the same flux crossed latitude 31°N between Madeira and Great Meteor Seamount uniformly, the northward drift would be less than 1 mm s^{-1} and hence unobservable. However, there is evidence in the paper cited that the northward flow is concentrated on the east margin of the basin, viz. west of Madeira, and is fed either from the south or west. If the margin flow were fed from the west an *eastward* current would result on the plain. Thus the observation at GME of a *westward* current suggests the flow on the margin is fed from the south.

An alternative estimate of the abyssal flow has been derived from the analysis of 10 CTD stations in the form of a triangle of side 500 km. The stations were made in the summer of 1983, six months before the current measurements at GME commenced (Saunders and Dolan 1987). On the very large scale of the CTD measurements it is supposed that changes are very slow, and the 3 years of deep current measurements show no evidence of secular change, even locally. The mean current profile is derived using the geostrophic relation along with estimates of the error (see Fig. 8). The indeterminacy of the origin of the profile has been removed by the two different β-spiral methods described by Coats (1981) and by Olbers et al. (1985). Here we shall merely note that both methods strive to ensure that (at each level considered)

1) the three-dimensional current vector lies on a stationary density surface, and
2) the north–south advection of planetary vorticity is balanced by vertical stretching.

Both solutions predict an eastward component of the flow at all levels with absolute minimum currents near 2500 db. The near-bottom velocity is ENE, slightly

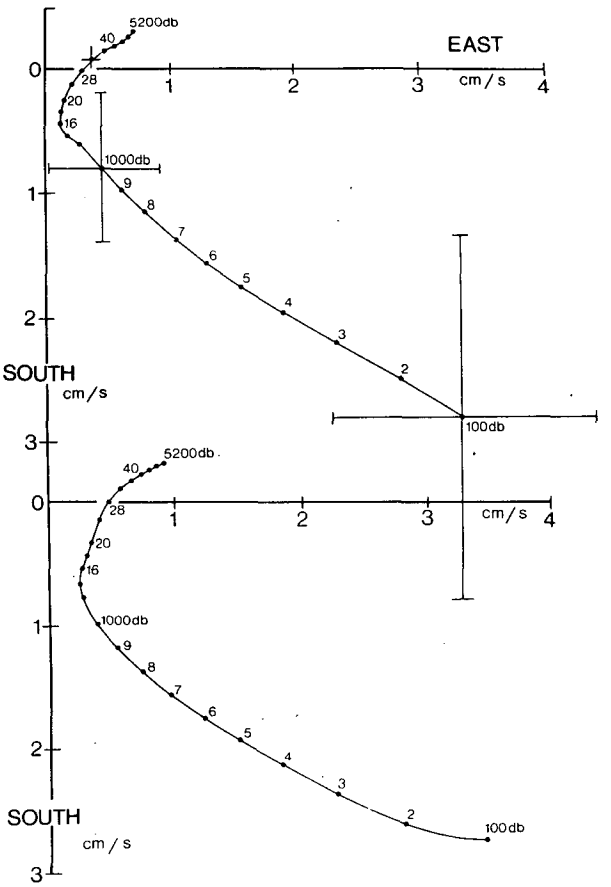

FIG. 8. Current profile derived from hydrographic data for region 30°–35°N, 21°–26°W. The origin is determined as indicated in the text; (upper) after Olbers et al. (1985) and (lower) after Coats (1981).

less than 1 cm s^{-1}, using both techniques. The method averages the result for the region covered by the stations, which is centered near 33°00′N, 23°30′W. The location of GME falls at the edge of the CTD triangle and is quite distant from its center, so that at first sight the discrepancy in mean direction is unremarkable. However recent concurrent two-year long measurements at 3000 m depth and at 32°N, 24°W (Schmitz et al. 1987) yield a mean current of 0.5 cm s^{-1} also to the west and earlier two-year long observations from NEADS1 at 33°N, 20°W (Dickson et al. 1985) yield a mean southwest current of 0.6 cm s^{-1}. Taken together these three measurements show that direct observations of currents and (deep) β-spiral estimates differ significantly. Either a "strong" eastward flow exists north of 33°N on the Madeira Plain or some assumption of the theory is violated.

In a study of the upper ocean in the Canary Basin, Käse et al. (1985, 1986) have shown the northern region to have a complex vigorous circulation. The eastward flowing Azores Current, which climatologically passes through the center of the triangle of observations

TABLE 4. Variance of low-passed currents at GME, $cm^2 s^{-2}$. Bold integers refer to number of successful deployments. Figures in parentheses are calculated with stalled rotor currents set zero.

Height above bottom (m)		Plain		Hill-foot		Hill-top	
10	East	4.28 (3.80)	3	3.18	2	3.64	3
	North	4.14 (3.60)		3.90		1.77	
1000	East	2.76 (2.36)	3	3.71	1	3.12	2
	North	2.74 (2.19)		2.71		2.04	

under consideration, was found to meander actively and shed eddies. Even when averaged spatially a density surface migrates appreciably and the nonstationarity of an individual realisation thus makes it inappropriate for a β-spiral analysis.

On the other hand, the β-spiral analysis of climatological data (Olbers et al. 1985), should avoid this objection. We are unable to present their hodograph here but find that at the deepest level of their analysis (2000 m) the current is approximately NE at 1–2 mm s^{-1}, compared with SE at 2–3 mm s^{-1} for our hodographs (Fig. 8). If the density field at levels deeper than 2000 m were stationary, the current shear derived from our data could be added to the Olbers et al. estimate of current to give a NE flow at abyssal depths, again at variance with the current meter data cited. Unfortunately we are unable to verify the (presumed) time dependence of the deep density field.

6. Low frequency variability of currents

A low-passed version of the data was prepared, by filtering and suppressing inertial and tidal frequencies. The variance of the east and north components at the long-term GME sites and at two depths is shown in Table 4.

On the plain the variance is isotropic and decreases with height above the seabed. At 10 m on the flank of the hill the variance of the east component is slightly reduced and on the hill-top the north component is considerably reduced. These directions represent the uphill components at the two sites; see also section 8. On the hill top there is little change in variance with height above seabed in contrast to the behaviour on the plain.

On the plain a 10%–20% reduction in variance results from setting the current speed zero when the instrument is stalled. A "best" estimate probably lies between the two values given but the small differences which are involved will be ignored since they do not affect any of the subsequent discussion.

Further distinctions are seen when the variance is separated into frequency bands by spectral analysis (Figs. 9 and 10), where a variance preserving presentation is employed. For the east component at both the plain and on the hill-top most of the energy is contained in the lowest band of frequencies (127–500 days). For the north component there is more variance in the second and third spectral bands (49–127 days) at both sites. The first band has been designated the "secular scale" and the second and third comprise most of the energy in the "temporary mesoscale" (Schmitz et al. 1987). The difference in the frequency content of the east and north components is quite evident in a plot of them (Fig. 11); the dominant frequency in the east component, at least on the basis of a few cycles, is not annual, in agreement with the finding of Dickson et al. (1985) that the annual cycle at abyssal depths is seen only at higher latitudes.

The two-year current record described by Schmitz et al. (1987), 100 km NE from GME, although it em-

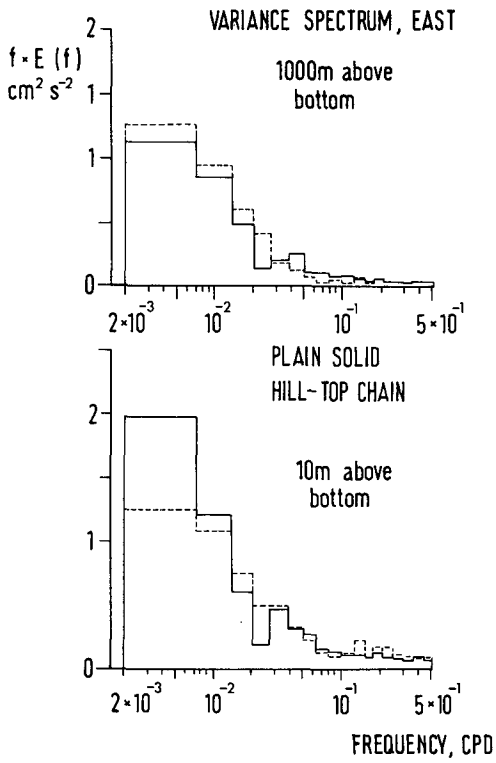

FIG. 9. Variance spectrum of east component of current 10 and 1000 m above and bottom: (solid) plain and (dashed) hill top.

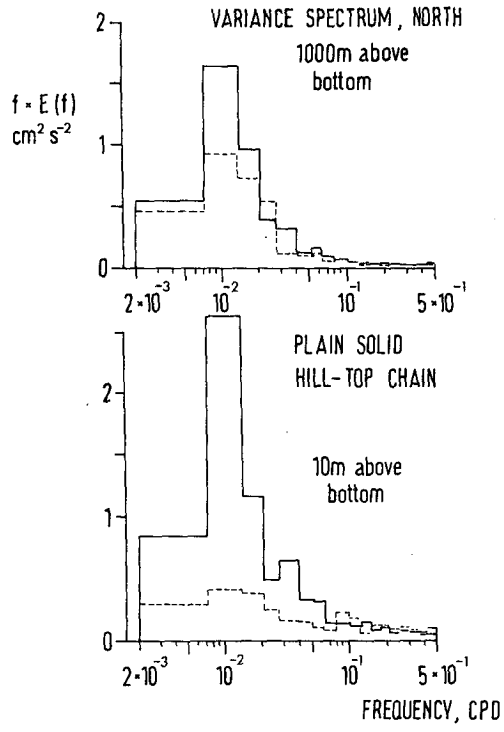

FIG. 10. Variance spectrum of north component of current 10 and 1000 m above bottom: (solid) plain and (dashed) hill top.

phasizes the upper part of the water column with the deepest instrument at 3000 m, provides some interesting contrasts. Schmitz et al. find that the mean of the east and north variance (eddy kinetic energy) exhibits a systematic shift from maximum energy at secular scale (127–500 days) at 500 m depth to maximum energy at the temporary mesoscale (49–127 days) at 3000 m depth. This tendency stated to be typical of open ocean locations is reversed at 5000 m depth in our data where the secular scale contains about 60% of the energy. The "redness" of the east variance is also found to be a property of shallow and thermocline depths disappearing at 3000 m yet reappearing strongly in the record at abyssal depths.

An alternative representation of the low-frequency variance is to be found by constructing a current ellipse in the manner used for tidal ellipses (Fig. 12). For the secular scale (127–500 days) the current ellipse is oriented east–west reflecting the excess of east variance over north. For the temporary mesoscale (49–127 days) the current ellipse(s) are oriented north–south reflecting the excess of north variance over east. A histogram of the frequency of current directions (not shown) also reveals the bimodality of E–W and N–S directions. Thus the bald assertion that the variance of currents on the plain is isotropic is seen to be quite misleading.

The above characteristics are suggestive of waves rather than eddies as a description of the current variability and this view is further supported by our estimates of the propagation of signals between the sites. First the coherence is computed between the currents on the plain on the same mooring, viz. at 10 and 1000 m above bottom. Coherence falls from very near unity at the longest periods to near zero at period of two days (not shown). The coherence is about 0.5 at a period of 7 days. The phase lag cannot be distinguished from zero. To estimate coherence errors we have used standard tables and to estimate phase errors we have used approximate expressions attributed to Jenkins (Priestley 1981). Thus current changes arrive simultaneously at the levels 10 and 1000 m above the plain.

Coherence has also been estimated between currents at the sites on the plain and on the hill-top (at 10 m height). Coherence magnitude falls to 0.5 at about 30-day period and the phase lag is nonzero for all coherences which differ significantly from zero (again not shown here). The phase is always negative implying the *westward* propagation of current change. From the phase angle, frequency, and separation, phase speed can be calculated. Phase speed varies between ~ 1 and 8 cm s^{-1}, increasing with decreasing period. Westward propagation and rectilinear current oscillation is a familiar property of planetary (Rossby) waves. The minimum phase speed of linear planetary waves in a stratified uniform-depth ocean for the same periods range between 0.6 and 15 cm s^{-1} (see Table 5). For periods less than 70 days the observed phase speed is less than the minimum and hence such disturbances are not of the Rossby wave character. Oscillations at longer pe-

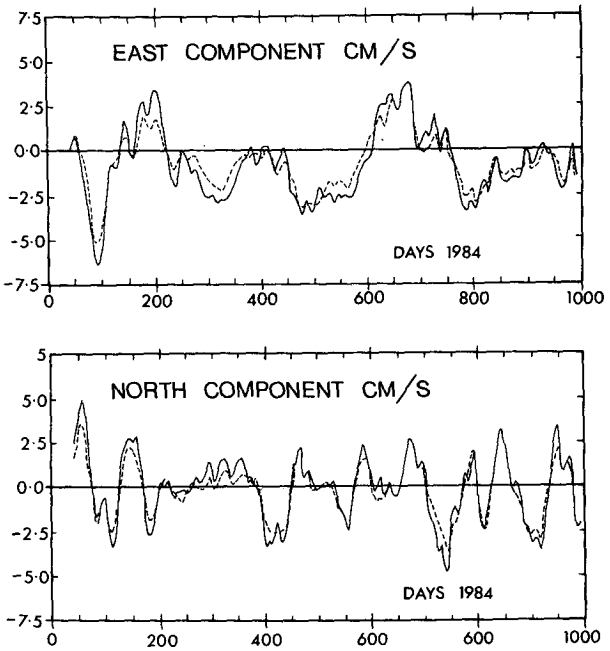

FIG. 11. Time series of current components on plain: origin is 1 Jan 1984. (Solid) 10 m a.b.; (dashed) 1000 m a.b.

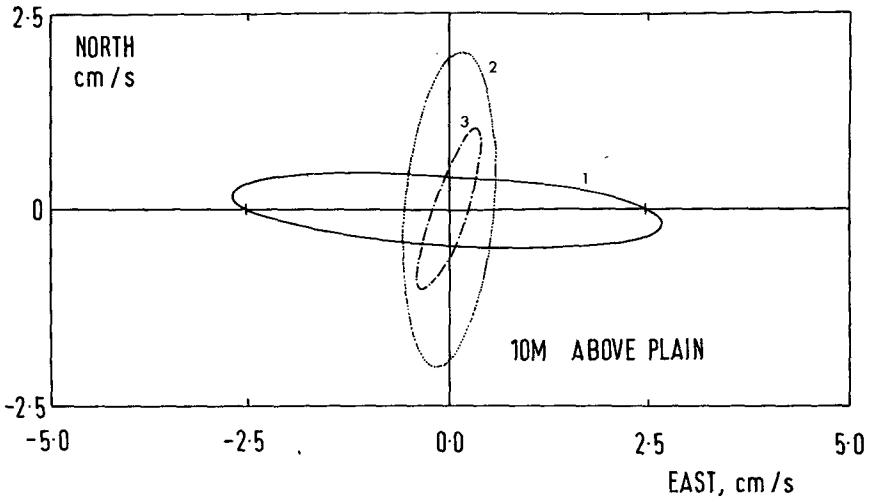

FIG. 12. Current ellipses for fluctuation with period 1: 127–500 days, period 2: 71–127 days and period 3: 49–71 days, measurements 10 m above plain.

riods are consistent with Rossby waves, although the orientation of the current ellipse for the first frequency interval (Fig. 12) suggest a nearly north–south propagating wave whose westward phase speed is no more than the minimum of 0.6 cm s^{-1} and has a wavelength in excess of 700 km. Even at secular scale periods (127–500 days), however, an examination of the GME and Schmitz et al. records about 100 km away reveals little evidence of coherence; thus, as has been demonstrated before, an explanation in terms of a single plane wave is generally quite unsatisfactory (McWilliams and Robinson 1974).

7. Horizontal dispersion at GME

The rate of mixing of a tracer by the fluctuating currents discussed in the previous section is determined by the energy of the flow and its Lagrangian integral time scale (Taylor 1921). This quantity is given by

$$I_L = \int_0^\infty C(\tau)d\tau$$

where $C(\tau)$ is the correlation function for a velocity component. As has been described elsewhere (Saunders 1983) the correlation function is "estimated" from current meter data so that diffusivity in the x, y directions is given by

$$K_x, K_y \approx I_E(u^2, v^2)$$

where u^2, v^2 are the variance in the x, y directions. The correlation function $[\overline{u(t)u(t+\tau)}]/u^2$ can be estimated directly from the data but, if this method is employed, the estimate of the integral time scale is found to be sensitive to the cutoff lag. To illustrate this the results for the two components of the current 10 m above the seabed on the plain are presented in Table 6. The east component, which has a red spectrum (Fig. 9) has its first zero crossing of the autocorrelation

TABLE 5. Coherence between currents on plain and hill-top.

Period (days)	Coherence		Phase (deg)	E–W measured phase speed (cm s^{-1})	Minimum phase speed (cm s^{-1})
127–318	E	0.90	−19 ± 11*	3.5 ± 1.9	0.6
	N	0.88	−50 ± 12	1.3 ± 0.35	(1.0)#
71–127	E	0.74	−34 ± 21	4.6 ± 3.0	3.3
	N	0.74	−70 ± 21	2.2 ± 0.4	
49–71	E	0.89	−45 ± 11	5.3 ± 3.8	8
	N	—			
37–49	E	0.70	−43 ± 24	7.7 ± 3.8	15
	N	0.73	−71 ± 22	4.7 ± 1.3	

* Uncertainty of phase—refer to text.
# First baroclinic mode: period exceeds 200 days and wavelength is 700–1000 km.

TABLE 6. Integral time scales derived from autocorrelation estimates on the Plain. The record length is 1000 days.

	East		North	
Zero crossing number	Time to zero crossing (days)	Integral (days)	Time to zero crossing (days)	Integral (days)
1	75	+28	25	+11
2	200	−10	75	−1
3			110	+2.5
4			150	−2.5
5			200	+4

function at 75 days and its second at 200 days. The integral time scale to these crossings is calculated as +28 days and −10 days, respectively. For the north component the zero crossings are at shorter intervals, as expected from its peaked spectrum (Fig. 10), and the oscillatory results for integration are shown in Table 6. Evidently the estimates of integral time scale are quite unreliable employing the direct method and reflect the lack of significance of the autocorrelation estimates after some fraction of the record length. Many authors integrate the correlation function to the first zero crossing. This almost certainly overestimates the integral time scale by a substantial factor but this truncation at least yields a positive quantity (as required).

The author favors a model-fitting approach, utilizing a damped cosine for the correlation function, viz.

$$C(\tau) = \cos\Omega\tau \exp(-\lambda\tau)$$

giving

$$I = \frac{\lambda}{\Omega^2 + \lambda^2}.$$

This form for the correlation function implies a normalized spectral density given by

$$E(f) = 2\lambda\left[\frac{1}{\lambda^2 + (\Omega + 2\pi f)^2} + \frac{1}{\lambda^2 + (\Omega - 2\pi f)^2}\right]$$

where f is cyclic frequency. Whether the expression for $C(\tau)$ or $E(f)$ is employed there are two constants λ, Ω with which to fit the data. Fitting the spectral density, Figs. 9 and 10, for the plain gives for the east component $2\pi/\Omega = 200$ days, $1/\lambda = 50$ days whence $I = 14$ days. For the north component $2\pi/\Omega = 95$ days, $1/\lambda = 35$ days whence $I = 6$ days. A similar fit of the spectral density exists for the east component of the hill-top data, but the north component is larger, $2\pi/\Omega = 200$, $1/\lambda = 15$, $I = 12$. Note these quantities are generally a factor of two smaller than the estimates obtained by integrating the autocorrelation function to the first zero crossing. Combining the model-fitted estimates of integral time scales with the variance from Table 4 gives horizontal (isopycnal) diffusivity values found in Table 7.

On the plain the diffusivities 100 m above the seabed are approximately 70% of the values at 10 m, and on the hill-top they are quite similar. The values tabulated here are between a factor of two and four higher than diffusivities previously reported (Saunders, 1983) on the abyssal plain. Consequently at this rate diffusion is likely to disperse a tracer over a basin, 1000 km on a side, in 5–10 years rather than the 20 years derived earlier (Saunders 1983). It will be noted that the hill-top values are indistinguishable from those for the plain. Probably abyssal hills have a larger impact on the vertical (diapycnal) diffusivity augmenting it in the flow separation processes which occur in the lee of the hill.

TABLE 7. Horizontal (isopycnal) diffusion by eddies (10 m above sea bed).

Site	Component	Integral time scale (days)	Variance ($cm^2\ s^{-2}$)	Diffusivity ($10^2\ m^2\ s^{-1}$)
Plain	E	14 ± 3	4.3	5.2
	N	6 ± 2	4.1	2.1
Hill-top	E	14 ± 3	3.6	4.3
	N	12 ± 3	1.8	1.9

8. Estimates of vertical velocity

Vertical velocity is the unobserved component of the total velocity vector. Not only may its measurement be diagnostic of non-linear process (Bryden 1976; Keffer 1983) but in the deep ocean it occupies a central role in determining the strength and direction of the abyssal circulation (Stommel 1958). Few attempts have been made to estimate vertical velocity directly at abyssal depths: the results of our efforts at GME are described in the following paragraphs.

Bryden (1976) pioneered the technique employed for the GME datasets. In short, conservation of (potential) temperature is assumed along with the thermal wind equation to relate vertical shear to horizontal temperature gradients. This latter relation requires in addition the existence of a locally well-defined temperature–salinity relation, which *is* found in the area (Saunders 1986). The equations used are a finite difference version of (2.1) and (2.5) of Keffer and include time dependent terms. The dataset consists of low-passed values of east, north, and temperature at 10 and 1000 m above the bottom, and the vertical velocity is estimated at midheight, viz. 500 m above bottom.

At the three long-term sites, time series of five-day average vertical velocity w have been constructed. The record means cannot be distinguished from zero but the rms fluctuation is largest at the hill-flank (230 days duration), intermediate at the hill top (625 days) and smallest on the plain (960 days). Values are presented in Table 8. Following Keffer (1983, Appendix A) we have estimated the rms error of w, σ_w, to be 0.7×10^{-2} cm s^{-1}, arising exclusively from the noise of an individual current measurement (0.5 cm s^{-1}). This number is very close to the value found for the plain site and is exceeded appreciably only at the hill foot.

Because the estimate of w is made quite close to the seabed it is appropriate to test the data against the kinematic boundary condition

$$w = -uh_x - vh_y$$

where h_x, h_y are the slope of the bottom in the east, north directions. The equation assumes no flow across the seabed and ignores the existence of any benthic boundary layer. Linear correlations between w and u,

TABLE 8. Linear regression of w on u (east) and v (north).

Site	σ_w (cm s^{-1})	Percent variance explained	$\frac{dw}{du} \times 10^{-3}$	$\frac{dw}{dv} \times 10^{-3}$	Upslope direction	Slope magnitude
Plain	0.8×10^{-2}	8$^+$	*	*	*	*
Hill-top	1.0×10^{-2}	50	−1.1	−6.1	190	6×10^{-3}
Hill-foot	1.5×10^{-2}	83	−9.6	2.2	285	1×10^{-2}

$^+$ Not statistically significant.

v have been determined for each of the three sites and the coefficients and the percentage of variance explained by the correlation are displayed in Table 8.

On the plain, w is uncorrelated with u and v, but at the hill top and at the hill foot the regression is significant and the upslope direction deduced is entirely compatible with the actual topography (Fig. 3). It is remarkable that the overall directions of the near-bottom *mean* flow, which have not been used in the analysis, are themselves at right angles to the upslope directions (namely 098° and 194°; see Table 3). The actual slope of the hill is about 10^{-1} but the value determined at the hill foot contains both an upstream effect and a vertical decay, since w is estimated at the level of the summit. The slope of the seabed in the 10 km around the plain site is no more than 3×10^{-4} and the expected contribution to the variance of w is therefore only 1%. The vertical velocity estimated from Ekman pumping ($h_E\zeta$) has about the same magnitude, viz. 10^{-3} cm s^{-1} and hence is also undetectable. It is encouraging that the topographic influences can be seen in estimates of w in the deep ocean but in order to infer vertical velocities away from topography a marked improvement in (horizontal) current measurements will need to be made.

Acknowledgments. The author wishes to thank Messrs Goy, Gwilliam, Moorey, Phillips, Smithers and Waddington for their assistance with CTD measurements and moored current meter observations; also the officers and crew of both the RVS *Charles Darwin* and RRS *Discovery* for their wholehearted assistance at sea. The contributions of Drs R. T. Pollard, W. J. Gould and J. C. Swallow, both at sea and ashore, are also gratefully acknowledged. This research was carried out both with the support of the Natural Environment Research Council and of the Department of the Environment as part of the latter's radioactive waste management research programme (under contract DoE, PECD7/9/216).

REFERENCES

Bendat, J. S., and A. G. Piersol, 1971: *Random Data, Analysis and Measurement Procedures.* Wiley-Interscience, 407 pp.

Bryden, H. L., 1976: Horizontal advection of temperature for low-frequency motions. *Deep-Sea Res.*, **23**, 1165–1174.

Coats, D. A., 1981: An estimate of absolute geostrophic velocity from the density field in the northeastern Pacific Ocean. *J. Geophys. Res.* **86**, 8031–8036.

Dickson, R. R., W. J. Gould, T. J. Muller and C. Mailliard, 1985: Estimates of the mean circulation in the deep (>2000 m) layer of the eastern North Atlantic. *Progress in Oceanography,* Vol. 14, Pergamon, 103–128.

Gould, W. J., R. Hendry and H. E. Huppert, 1981: An abyssal topographic experiment. *Deep-Sea Res.*, **28**, 409–440.

Huppert, H. E., 1975: Some remarks on the initiation of inertial Taylor columns. *J. Fluid. Mech.*, **67**, 397–412.

——, and K. Bryan, 1976: Topographically generated eddies. *Deep-Sea Res.*, **23**, 655–680.

Käse, R. H., W. Zenk, T. B. Sanford and W. Hiller, 1985: Currents, fronts, and eddy fluxes in the Canary Basin. *Progress in Oceanography,* Vol. 14, Pergamon, 231–257.

——, J. F. Price, P. L. Richardson and W. Zenk, 1986: A quasi-synoptic survey of the thermocline circulation and water mass distribution within the Canary Basin. *J. Geophys. Res.*, **91**, 9739–9748.

Keffer, T., 1983: Time-dependent temperature and vorticity balances in the Atlantic North Equatorial Current. *J. Phys. Oceanogr.*, **13**, 224–239.

McWilliams, J. C., and A. R. Robinson, 1974: A wave analysis of the Polygon array in the tropical Atlantic. *Deep-Sea Res.*, **21**, 359–368.

Olbers, D. J., M. Wenzel and J. Willebrand, 1985: The inference of North Atlantic circulation patterns from climatological hydrographic data. *Rev. Geophys.*, **23**, 313–356.

Owens, W. B., and N. G. Hogg, 1980: Oceanic observations of stratified Taylor columns near a bump. *Deep-Sea Res.*, **27**, 1029–1045.

Preistley, M. B., 1981: Multivariate series, prediction and control. *Spectral Analysis and Time Series, Vol. 2,* Academic Press, 890 pp.

Saunders, P. M., 1983: Benthic observations on the Maderia abyssal plain: Currents and dispersion. *J. Phys. Oceanogr.*, **13**, 1416–1429.

——, 1986: The accuracy of measurements of salinity, oxygen and temperature in the deep ocean. *J. Phys. Oceanogr.*, **16**, 189–195.

——, 1987a: Currents, dispersion and light transmittance measurements on the Madeira abyssal plain. IOS Rep. No. 241, 55 pp.

——, 1987b: Flow through Discovery Gap. *J. Phys. Oceanogr.*, **17**, 631–643.

——, and J. W. Cherriman, 1983: Abyssal temperature measurements with Aanderaa current meters. *Deep-Sea Res.*, **30**, 663–667.

——, and F. Dolan, 1987: CTD data from Discovery Gap and the Madeira abyssal plain. IOS Rep. No. 236, 76 pp.

Schmitz, W. J., P. L. Richardson and J. F. Price, 1987: Recent sofar float and moored current meter observations in the Eastern Atlantic near 32°N. *J. Mar. Res.*, in press.

Searle, R. C., P. J. Schultheiss, P. P. E. Weaver, M. Noel, R. B. Kidd, C. L. Jacobs and Q. J. Huggett, 1985: Great Meteor East (Distal Maderia Abyssal Plain): Geological studies of its suitability for disposal of heat-emitting radioactive wastes. IOS Rep. No. 193, 161 pp.

Stommel, H., 1958: The abyssal circulation. *Deep-Sea Res.*, **5**, 80–82.

Taylor, G. I., 1921: Diffusion by continuous movements. *Proc. London Math. Soc.*, **A20**, 196–211.